

Comparison of Tunneling Characteristics in the MTJs of CoFeB/MgO/CoFeB with Lower and Higher Tunneling Magnetoresistance

G. M. Choi¹, K. H. Shin¹, S. A. Seo², W. C. Lim³, and T. D. Lee^{3*}

¹Center for Spintronics Research, KIST, Seoul 136-791, Korea

²Semiconductor Device Lab, Samsung Advanced Institute of Technology, Yongin 446-712, Korea

³Department of Materials Science & Engineering, KAIST, Daejeon 305-701, Korea

(Received 21 November 2008, Received in final form 18 February 2009, Accepted 11 March 2009)

We investigated the I - V curves and differential tunneling conductance of two, CoFeB/MgO/CoFeB-based, magnetic tunnel junctions (MTJs): one with a low tunneling magnetoresistance (TMR; 22%) and the other with a high TMR (352%). This huge TMR difference was achieved by different MgO sputter conditions rather than by different annealing or deposition temperature. In addition to the TMR difference, the junction resistances were much higher in the low-TMR MTJ than in the high-TMR MTJ. The low-TMR MTJ showed a clear parabolic behavior in the dI/dV - V curve. This high resistance and parabolic behavior were well explained by the Simmons' simple barrier model. However, the tunneling properties of the high-TMR MTJ could not be explained by this model. The characteristic tunneling properties of the high-TMR MTJ were a relatively low junction resistance, a linear relation in the I - V curve, and conduction dips in the differential tunneling conductance. We explained these features by applying the coherent tunneling model.

Keywords : magnetic tunnel junction, MgO barrier, tunneling magnetoresistance

1. Introduction

Magnetic tunnel junctions (MTJs) are composed of a thin insulating barrier sandwiched between two ferromagnetic electrodes. The tunneling conductance of MTJs is dependant on the magnetization configurations of the two adjacent ferromagnetic electrodes. The conductance becomes high at a parallel configuration (P) and low at an anti-parallel configuration (AP). The amount of this conductance change is called the tunneling magnetoresistance (TMR), which has conventionally been explained by the simple barrier model established by Simmons [1]. However, the recently developed, Fe(001)/MgO(001)/Fe(001)-based MTJs could not be explained by this model, because tunneling conductance is determined by the coherent tunneling mechanism associated with the symmetry of Bloch states and the complex band structures of MgO (001) and Fe (001) [2, 3].

In this work, we have compared the I - V curves and differential tunneling conductance between the low-TMR (22%) and high-TMR (352%) MTJs. We achieved the

low and high TMR properties merely by changing the MgO sputter conditions rather than by changing the post-annealing [4] or deposition [5] temperature. The high junction resistance and nonlinear behavior of the I - V curve of the low-TMR MTJ were well explained by the simple barrier model. However, the relatively low junction resistance and nearly linear behavior in the I - V curve of the parallel state of the high-TMR MTJ were better explained by the coherent tunneling model than by the simple barrier model. Especially, conduction dips at $\sim \pm 390$ mV in differential tunneling conductance were only observed in the high-TMR MTJ. We attributed this conduction dip to the Bloch states of the coherent tunneling model.

2. Experimental Procedures

MTJs were made by a magnetron sputtering system with a base pressure of 5×10^{-9} Torr. Ta/NiFe/IrMn/CoFe/Ru/CoFeB/MgO/CoFeB/Ta stacks were deposited on oxidized Si and fabricated to $10 \mu\text{m} \times 10 \mu\text{m}$ cells by photolithography and ion beam etching. We used a $\text{Co}_{40}\text{Fe}_{60}$ alloy for CoFe and a $(\text{Co}_{40}\text{Fe}_{60})_{80}\text{B}_{20}$ alloy for CoFeB.

*Corresponding author: Tel: +82-42-350-3336
Fax: +82-42-350-5310, e-mail: tdlee@kaist.ac.kr

The low-TMR (sample A) and high-TMR (sample B) MTJs had the same MgO thickness (2 nm) and the same post-annealing temperature of 400°C for 1 hr. The only difference between the two samples was the MgO sputter conditions. For samples A and B, MgO was deposited at an Ar pressure of 1 and 10 mTorr, rf power of 60 and 100 W, target-to-substrate distance of 5 and 5 cm, and substrate bias of 0 and –20 V, respectively. Detailed deposition conditions have been presented elsewhere [6]. TMR and I - V curves for the P and AP configurations were measured at room temperature by a d.c. two-point probe method. The TMR curves were obtained by measuring the voltages while changing the magnetic field at a constant applied current. The I - V curves were obtained by measuring the voltages while changing the current at a constant magnetic field. The tunneling spectra were represented by differential tunneling conductance (dI/dV as a function of V) which was obtained mathematically from the measured I - V curves.

3. Results and Discussion

Fig. 1 shows the TMR results of samples A and B, with TMR values of 22% and 352%, respectively, at the applied current of 1 μ A. From the insets of Fig. 1, the highest TMR values were \sim 30% in sample A and \sim 400% in sample B at the zero bias voltage. Even though their MgO thickness and post-annealing temperature were the same, the TMR values differed greatly. The Resistance-area product (RA) values at a P configuration were much higher in sample A than in sample B, despite the same MgO thickness. The TMR dependency on the bias voltage also differed between the two samples, as shown in the insets of Fig. 1. The voltage where TMR dropped to half of the maximum was around 200 and 400 mV in samples A and B, respectively. Several possible reasons are proposed to account for these different tunneling properties. Firstly, the quality of MgO (001) growth, which is essential for a high TMR [2, 3] must have been different. X-ray diffraction (XRD) analysis revealed that the MgO (002) peak intensity was much bigger for the MgO deposition conditions of sample B than for those of sample A, as shown in Fig. 1(c), suggesting that the MgO barrier in sample B had sharper (001) textures. Secondly, oxidation of the bottom CoFeB electrode or intermixing of MgO with the bottom electrode may have affected the conduction properties. Since MgO was deposited at much lower Ar pressure in sample A than in sample B, the sputtered atoms will have arrived at the substrate with higher kinetic energy in the case of sample A, thereby leading to oxidation of the bottom electrode or intermix-

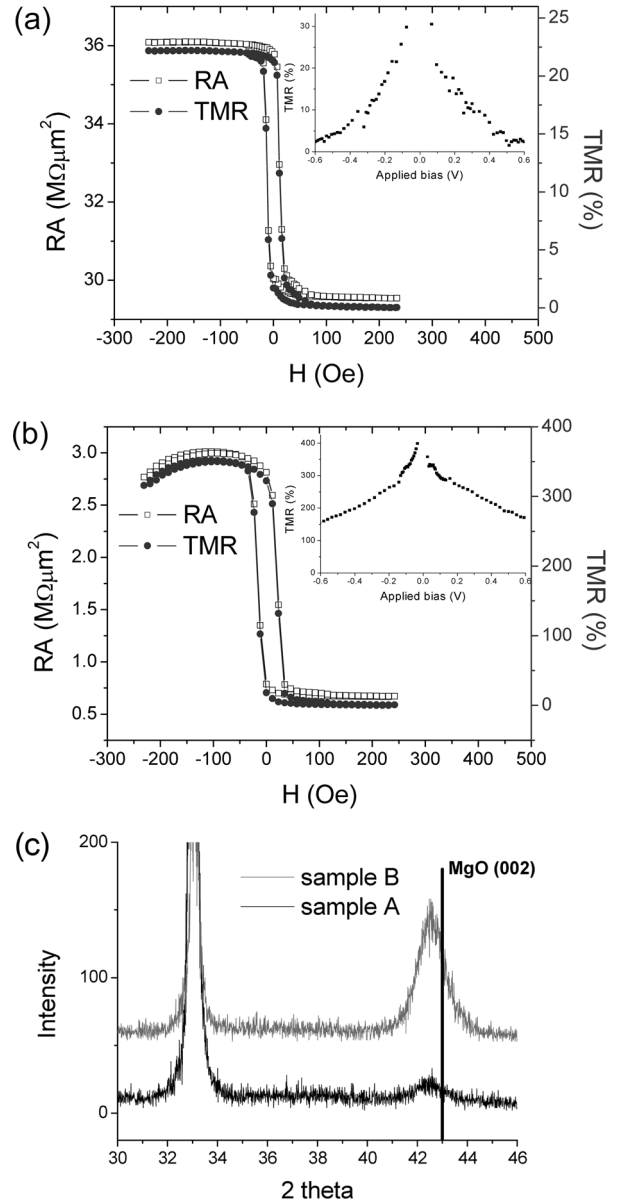


Fig. 1. TMR and RA results of samples A (a) and B (b). The insets show the bias dependency of TMR. The MgO (002) peak intensity of Ta(5 nm)/CoFeB(5 nm)/MgO(10 nm) at the as-deposited state (c).

ing with bottom electrode materials. Recent reports have shown that B, Fe, and Co oxides form at the CoFeB/MgO interface in a sputtering process [7, 8]. In addition, a recent report has claimed that different vacancy concentrations in the barrier due to the different MgO deposition conditions can affect the conductance properties [5].

The large difference in tunneling behaviors implied some variation in tunneling mechanisms between samples A and B. To verify the tunneling mechanism, we fitted the I - V curves of a parallel state with Simmons' equation

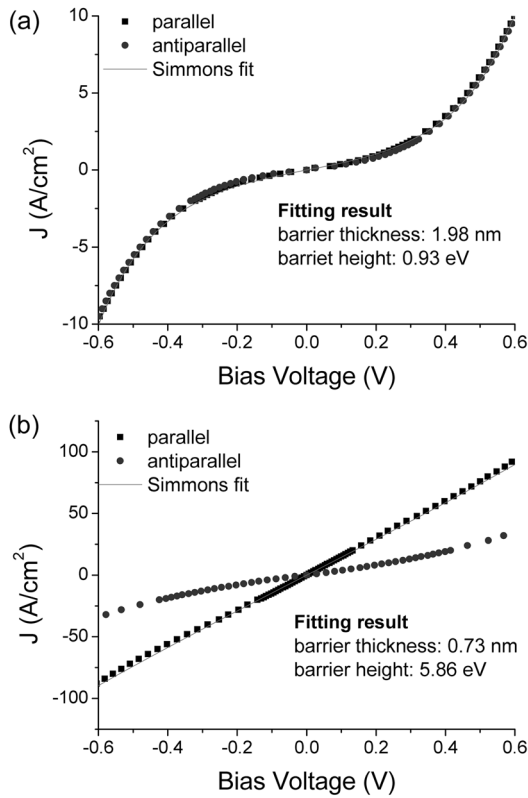


Fig. 2. I - V curves of samples A (a) and B (b). Simmons' fitting results for parallel state, I - V data are shown within the figure.

and the results are shown in Fig. 2. Sample A exhibited a barrier thickness of 1.98 nm and a barrier height of 0.93 eV. The former was nearly the same as the deposited MgO thickness and the latter was also reasonable because the barrier height of MgO could be lower than 1.2 eV due to the oxygen vacancy state [9]. However, the fitted result of sample B was not realistic because the calculated MgO thickness was 0.73 nm, which was far smaller than 2 nm. The very high TMR of sample B was indicative of a coherent tunneling mechanism. If the tunneling mechanism is governed by coherent tunneling, then the expected value for RA at the MgO thickness of 2 nm would be 1~10 k Ω um² (from Fig. 16 in reference [2]). Even though the RA of sample B (~670 k Ω um²) was much lower than that of sample A, it was much higher than the reference value, which was attributed to a thicker MgO thickness or local oxidation of some parts of the bottom electrode. More detailed discussion on the RA values of the MgO barrier can be found in Gibson *et al.* [10].

Fig. 3 shows the differential tunneling conductance of the parallel state as a function of bias voltages in samples A and B. In both samples, the conduction was higher at positive bias voltages. At positive bias voltages, the current

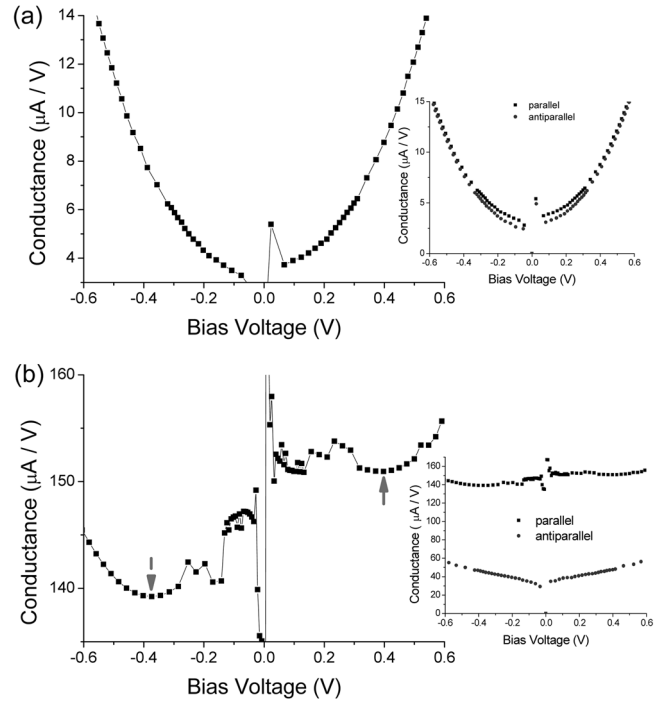


Fig. 3. Differential tunneling conductance as a function of bias voltage of a parallel state for samples A (a) and B (b). The arrows in (b) indicate conduction dips at $\sim\pm 390$ mV. The insets show the whole differential tunneling conductance with a parallel state and an anti-parallel state.

flows from the top electrode to the bottom electrode, while electrons flow from the bottom to the top. This implies the presence of asymmetry at the interfaces of the top and bottom electrodes with the MgO barrier. The quality of these interfaces can be affected by misfit dislocations, elastic strain, electrode oxidation, or intermixing of atoms. In sample B, there were conduction dips at $\sim\pm 390$ mV, as shown in Fig. 3(b). Many research groups have reported conduction dips at 300~400 mV [4, 11, 12, 13], and several of them explained this phenomena with Bloch states of the coherent tunneling model. Because sample A, in which the tunneling properties are explained by the simple barrier model, does not show any conduction dip, we attributed this conduction dip in sample B with the Bloch states of the coherent tunneling. The conduction dip was clear in the parallel state but not clear in the anti-parallel state. In a parallel state, conduction is mostly made by majority carriers, and the tunneling conductance can be written in terms of its transmission coefficient [2]:

$$G = \frac{e^2}{h} \sum_{k_{||}, j} T^+(k_{||}, j)$$

where T^+ is the transmission coefficient, $k_{||}$ the wave vector

parallel to the layer, and j the different Bloch states. While in the body centered cubic (bcc) Fe structure, the majority carriers have Δ_1 , Δ_5 and Δ_2 Bloch states, in the bcc Co and bcc CoFe alloys, the majority carriers only have the Δ_1 Bloch state [14, 15]. Therefore, the conductance of the majority carriers in the parallel state of the bcc CoFeB alloy will be

$$G = \frac{e^2}{h} \sum_{k_{||}} T_{\Delta_1}^+(k_{||})$$

When the Fermi level is lowered to a critical level by applied biases, the Δ_5 and Δ_2 Bloch states also tunnel through the barrier and the conductance will be

$$G = \frac{e^2}{h} \left\{ \sum_{k_{||}} T_{\Delta_1}^+(k_{||}) + \sum_{k_{||}} T_{\Delta_5}^+(k_{||}) + \sum_{k_{||}} T_{\Delta_2}^+(k_{||}) \right\}$$

Because of the additional Bloch states, the majority carrier conductance may start to increase at a critical bias voltage. Therefore, we attributed this conduction dip in sample B to the participation of the Δ_5 and Δ_2 states in conduction. From the Fig. 1(b) of reference [14], the energy difference between the Fermi level and the top of the Δ_5 and Δ_2 Bloch states was ~ 0.58 eV in the bcc Co. However, this energy difference in the CoFeB alloy has not been reported. Based on the study results presented here, we assert that this energy difference of the $(\text{Co}_{40}\text{Fe}_{60})_{80}\text{B}_{20}$ alloy is ~ 0.39 eV.

4. Conclusion

We have compared the tunneling properties of two CoFeB/MgO/CoFeB MTJs: low-TMR and high-TMR. Both MTJs were fabricated in the same conditions except for the MgO deposition conditions. The tunneling properties of the low-TMR MTJ were well explained by Simmons' simple barrier model, while those of the high-TMR MTJ could not be explained by this model and were better explained by the coherent tunneling model. Since conduction dips were not observed in the MTJ whose tunneling properties were well explained by Simmons' simple barrier model, we attributed the conduction dips in the high-TMR MTJ to the Bloch states of the coherent tunneling model. The increase in the tunneling conductance with the availability of additional Bloch states suggested that the energy difference between the Fermi level and the top of the Δ_5 and Δ_2 Bloch states is ~ 0.39 eV in the $(\text{Co}_{40}\text{Fe}_{60})_{80}\text{B}_{20}$ alloy. Similar differences of tunneling properties depending on either the annealing temperature, which affects the crystallization of electrodes, or the deposition temperature, which affects the amount of oxygen

vacancies in the MgO barrier, have been observed by other groups. In the present study, we varied the tunneling properties by applying different MgO sputter conditions, which, based on the XRD analysis, seemed to affect the MgO (001) growth quality.

Acknowledgment

This work was supported by the National Program for Tera-level Nanodevices of the Korea Ministry of Science and Technology as a 21st Century Frontier Program.

References

- [1] J. G. Simmons, *J. Appl. Phys.* **34**, 1793 (1963).
- [2] W. H. Butler, X.-G. Zhang, T. C. Schulthess, and J. M. Maclaren, *Phys. Rev. B* **63**, 054416 (2001).
- [3] J. Mathon and A. Umerski, *Phys. Rev. B* **63**, 220403(R) (2001).
- [4] R. Matsumoto, S. Nishioka, M. Mizuguchi, M. Shiraishi, H. Maehara, K. Tsunekawa, D. D. Djayaprawira, N. Watanabe, Y. Otani, T. Nagahama, A. Fukushima, H. Kubota, S. Yuasa, and Y. Suzuki, *Solid State Comm.* **143**, 574 (2007).
- [5] G. X. Miao, Y. J. Park, J. S. Moodera, M. Seibt, G. Eilers, and M. Müntenberg, *Phys. Rev. Lett.* **100**, 246803 (2008).
- [6] G. M. Choi, K. H. Shin, S. A. Seo, S. O. Kim, W. C. Lim, and T. D. Lee, Proceedings for publication in IEEE Transactions on Magnetics as a contributed paper in Asian magnetic Conference, 10 December, 2008, Busan, South Korea, Abstract BA-05.
- [7] J. Y. Bae, W. C. Lim, H. J. Kim, D. J. Kim, K. W. Kim, T. W. Kim, and T. D. Lee, *J. Magnetism* **11**, 25 (2006).
- [8] J. C. Read, P. G. Mather, and R. A. Buhrman, *Appl. Phys. Lett.* **90**, 132503 (2007).
- [9] A. Gibson, R. Haydock, and J. P. LaFemina, *Phys. Rev. B* **50**, 2582 (1994).
- [10] T. Nagahama and J. S. Moodera, *J. Magnetism* **11**, 170 (2006).
- [11] G.-X. Miao, K. B. Chetry, A. Gupta, W. H. Butler, K. Tsunekawa, D. Djayaprawira, and G. Xiao, *J. Appl. Phys.* **99**, 08T305 (2006).
- [12] R. Matsumoto, Y. Hamada, M. Mizuguchi, M. Shiraishi, H. Maehara, K. Tsunekawa, D. D. Djayaprawira, N. Watanabe, Y. Kurosaki, T. Nagahama, A. Fukushima, H. Kubota, S. Yuasa, and Y. Suzuki, *Solid State Comm.* **136**, 611 (2005).
- [13] Y. Jang, C. Nam, K.-S. Lee, B. K. Cho, Y. J. Cho, K.-S. Kim, and K. W. Kim, *Appl. Phys. Lett.* **91**, 102104 (2007).
- [14] S. Yuasa, A. Fukushima, H. Kubota, Y. Suzuki, and K. Ando, *Appl. Phys. Lett.* **89**, 042505 (2006).
- [15] X.-G. Zhang and W. H. Butler, *Phys. Rev. B* **70**, 172407 (2004).